Analyst

Convection-driven microfabricated hydrogels for rapid biosensing

Journal:	*Analyst*
Manuscript ID	AN-COM-05-2020-001069.R2
Article Type:	Communication
Date Submitted by the Author:	12-Aug-2020
Complete List of Authors:	Cheng, Cheng; University of Wyoming, Chemical Engineering Harpster, Mark; University of Wyoming, Chemical Engineering Oakey, John; University of Wyoming, Chemical Engineering

COMMUNICATION

Convection-driven microfabricated hydrogels for rapid biosensing

Cheng Cheng, Mark H. Harpster and John Oakey *

Received 00th January 20xx,
Accepted 00th January 20xx

DOI: 10.1039/x0xx00000x

A microscale biosensing platform using rehydration-mediated swelling of bio-functionalized hydrogel structures and rapid target analyte capture is described. Induced convective flow mitigates diffusion limited incubation times, enabling model assays to be completed in under three minutes. Assay design parameters have been evaluated, revealing fabrication criteria required to tune detection sensitivity.

Introduction

The development of rapid immunoassay platforms continues to enable point of care diagnostics for disease diagnostics and prognostic monitoring.[1] The urgency to find effective, simple, low cost, accurate, and rapid tests has been recently highlighted as a particularly urgent and unmet need. [2, 3] A variety of immunoassays and ligand recognition assays have being proposed and developed for environmental monitoring and medical diagnostics, including enzyme-linked immunosorbent assays (ELISA)[4, 5], Surface-enhanced Raman Spectroscopy (SERS),[6, 7] and paper-based microfluidic immunoasssays.[8, 9] Nevertheless, these approaches all suffer from different limitations. For example, ELISA requires high sample volumes and tedious and time consuming laboratory procedures.[10] SERS suffers from long pre-incubation and concentration steps needed to generate a strong, detectable signal.[11] As for paper-based assays, homogeneous sample concentration is limited by the inability to spatially localize imbibition. Therefore, there remains an acute need to develop rapid and reliable molecular recognition and immunoassy platforms that can be delivered at the point of care. Introducing and utilizing inexpensive and versatile materials has the potential to significantly broaden the reach of biosensing platforms.

In recent years, hydrogel matrices have been developed as a central enabling technology for diverse biomedical applications[12,13,14] Consisting of macromolecular networks derived from the polymerization and cross-linking of diversely reactive macromers (e.g. poly(acrylic acid),[15] poly(vinylpyrrolidone)[16] and poly(ethylene glycol)-based))[17, 18] that swell and demonstrate high solubility in aqueous solutions, their well-recognized biocompatibility,[19,20] ease in micro-patterning their fabrication,[21,22,23,24] as well as advancements in the chemical derivatization of reactive macromers for tailored polymer chemistries,[25,26,27] have fostered significant progress in demonstrating the flexibility of hydrogels for precisely tuning desired physical, mechanical, and chemical properties. The functionalization of hydrogels with biomolecules, in particular, has enabled their effective utilization as biomimetic scaffolds for cell and tissue growth,[28,29] encapsulants for controlled drug delivery, [30,31] and versatile biosensors for cell,[32] protein, antibody, nucleic acid, and microbe detection.[33,34]

Due to their flexibility, hydrogels undergo osmotic-driven conformational changes in structure (i.e. swelling and shrinkage), the extent of which is dictated by the respective degree of cross-linking and charge density of the polymer matrix.[35] Utilizing hydrogel's acute responsiveness to changes in the local aqueous environment, along with the capability to precisely engineer the mesh, or pore, distribution size for enabling analyte uptake or exclusion,[36,37] a broad spectrum of sensing platforms have been developed. Park *et al.*[38] and Al-Ameen *et al.*[39], for instance, have reported the fabrication of distinctly shaped macroporous hydrogel particles, each of which was functionalized with antibodies (Ab)s specific for the recognition of a clinically relevant antigen. Following incubation in a sandwich-type assay with antigen mixtures and reporter Abs conjugated to the same fluorophore, multiplex detection and high level detection sensitivity was demonstrated by the specificity and intensity of the different fluorescing shapes. In other sandwich-type immuno-sensing applications, nanocomposite hydrogels consisting of Ab-functionalized polystyrene beads immobilized in macroporous hydrogel scaffolds have been developed as a means of enhancing detection sensitivity by increasing the effective surface area available for antigen capture.[40,41] Using arrays of nanocomposite hydrogel droplets, Li *et al.*[42] demonstrated a multiplex detection capability for 6 disease biomarkers commonly found in human serum and a limit of detection sensitivity of ~1 pg/mL. Relying exclusively on the capability of monitoring the equilibrium swelling state of hydrogels, there are also several reports of functionalized "smart gels" that have been shown to be highly responsive and sensitive to the introduction

*Department of Chemical Engineering
University of Wyoming
Laramie, WY 82070
Electronic Supplementary Information (ESI) available: [details of any supplementary information available should be included here]. See DOI: 10.1039/x0xx00000x

of sequence complementary target DNAs,[43] changes in glucose levels,[44] temperature[45], pH[45] and a host of physical stimuli. [46,47,48]

While phase transitions in the hydration state of hydrogels have been exploited for developing a broad spectrum of actuators,[35,49,50] the transition that occurs from the dehydrated state to full hydration, and vice-versa, has attracted limited attention. Lyophiized spotted arrays of IgG-frunctionalized hydrogels developed for high-throughput sandwich immunoassays, for instance, were developed for convenience and long-term storage of antigen capture scaffolds.[51] Using dehydrated hydrogel scaffolds containing immobilized Au and Ag nanoparticles previously incubated with a Raman-active pesticide, a strong surface-enhanced Raman effect was reported.[51] Here, drying and collapse of the hydrated hydrogel matrix served to concentrate captured pesticide within the collective surface metal plasmon resonances induced by laser excitation, thereby greatly increasing the intensity of the Raman signaling and detection sensitivity. In a functionally similar approach, Lifson *et al.*[52] have reported on the incubation of TNF-α antigen with hydrated acrylamide scaffolds functionalized with anti-TNF-α Abs and spotted on silicon wafers, after which the capture complex was dried and analyzed by array imaging reflectrometry. Detection sensitivities as low as 1 pg/mL were recorded based on measured increases in wafer thickness. While high-level detection sensitivity was achieved in both cases, instrumentation requirements and the lengthy times required to dry assay reactions are impractical for onsite or point of care test applications.

In an effort to explore the potential of hydrogel hydration states and rehydration specifically as an enabling mechanism for rapid analyte detection, we describe feasibility studies using a model fluorometric rehydration assay consisting of surface functionalized hydrogel micropillars in which analyte capture and detection is achieved within less than a minute following incubation with analyte-containing solution. The rates of recorded recognition are significantly faster than what is typically reported for immunoassays in the literature and shown to be a direct consequence of rehydration-mediated convective flow, which effectively overcomes the slow rates of diffusive mass transfer and capture surface/analyte interaction in solutions of biomolecules with small diffusion coefficients .[53,54] While efforts to model the efficacies of particle-based biosensors in reducing analyte recognition times have identified critical experimental design parameters impacting assay performance,[55,56] actual recorded assay times range from several minutes to several hours and often require complex procedures and instrumentation for conducting assays and data processing.[57,58,59,60] In the present study, the preliminary characterization of critical assay design features and their impact on assay performance metrics provide feaibility for a strategy that enables a novel and facile analyte sensing platform that provides high-level detection sensitivity with fast reaction times on the order of minutes.

Materials and Methods

Chemicals/biologicals

Ethanol, dimethyl sulfoxide (DMSO), 10X phosphate buffered saline (PBS), 3-(trimethyloxysilyl)propyl acetate, ethanolamine, biotin, ovalbumin, β lactoglobulin A and heterobifunctional Acrylate-PEG-*N* hydroxysuccinimide (AC-PEG-NHS) (M_w 5 kDa) were purchased from Sigma Aldritch (USA). Neutravidin, NHS-rhodamine and glass slides were purchased from Thermo Fisher Scientific (USA). Homobifunctional PEG diacrylate (PEGDA 700) (M_w 700 Da) and heterobifunctional Acrylate-PEG-Biotin (AC-PEG-Biotin) (M_w 2 kDa) was purchased from Jenkem Technology (USA) and Nanocs (USA), respectively. Polydimethylsiloxane (PDMS) was purchased from Ellsworth Adhesives (USA) as a kit containing viscous elastomer (part A) and curing cross-linker (part B). Recombinant protein A/G (pA/G) was purchased from Prospec (Israel) and superoxide dismutase was purchased from Worthington Chemicals (USA). SU-8 50 epoxy photoresist and silicon wafers were obtained from MicroChem (USA) and Silicon Inc. (USA), respectively. Rabbit pre-immune serum used to prepare enriched IgG by protein A/G agarose affinity chromatography (Thermo Fisher Scientific) was the kind gift of USDA/ABADRU (Manhattan, KS). Lithium phenyl-2,4,6-trimethylbenzolylphosphinate (LAP) was synthesized as previously described [61] according to the methodology of Majima et al.[62]

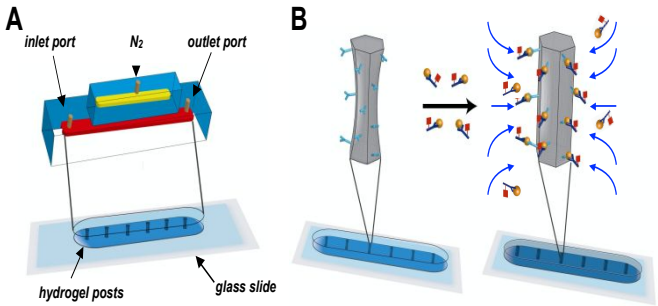

Figure 1 (A) Rendering of PDMS/glass chamber device used for convective flow assay demonstrations. (B) Schematic of sandwich-type immunoassay depicting rehydration-mediated convective flow delivery of target antigen/reporter complex to Ab-functionalized hydrogel post structure. Following rapid filling of the channel, the sample solution reaches quiescence around the dehydrated hydrogel pillars. As sample fluid is drawn to hydrogel surfaces during pillar rehydration, the solution contents are concentrated and retained at the interface.

Fabrication of PDMS chambers/hydrogel micropillar fabrication

Using standard soft lithography procedures ,[63] PDMS chambers were fabricated by first mixing PDMS solution and curing agent to a 10:1 ratio, which was then applied to a SU-8 50 micropatterned silicon wafer and cured overnight in a 70°C oven. Following removal of the PDMS replicate (channel dimensions: 220 µm (*h*) x 3000 µm (*w*) x 5000 µm (*l*)), inlet and outlet ports were punched using a 20 G needle, after which the chamber was sealed by bonding to an acrylated glass slide previously immersed in 3-(trimethoxysilyl)propyl acetate, washed with EtOH and then dried. A second, single inlet deadheaded chamber was bonded upon the first device and connected to pressurized nitrogen. The role of this chamber was solely to facilitate the fabrication of more uniform pillars [24], and was not employed subsequent to fabrication. Hydrogel pillars, or posts, were fabricated injecting 30 µl of prepolymer solution (chamber volume) consisting of 0.02% (w/w) of the photoinitiator LAP, 20% (w/w) PEGDA 700 and varying concentrations of either AC-PEG-Biotin or AC-PEG-NHS. The chamber was then placed with the glass slide down on the platform of an Olympus IX81 microscope fitted with a Polygon400 multiwavelength spatial illuminator (Mightex,

Canada), upon which the selected UV light pattern was projected (10 s, 20X lens/1.6 mW/cm^2) and controlled for post fabrication using integrated PolyScan software. Metamorph software (Molecular Devices, USA) was used for imaging and control of platform movement. Following post fabrication, the glass slide was removed and chamber flushed with PBS, followed by EtOH. Following post fabrication, the glass slide was removed from the chamber, air-dried overnight and then reattached to the PDMS chamber for conducting convective flow assays.

Fluorescent image acquisition/analysis

Fluorescent images were acquired using a 100W Hg lamp and Olympus U-MNG cube with a band pass filter for excitation, and a long pass BA590 barrier filter for red emission detection. Images were recorded using Q-Capture Pro 7 software (Qimaging, USA) control of a Q-Color5 digital camera imaging system (Olympus). Confocal microscopy was performed using a Zeiss LSM 710 laser scanning microscope (561 nm laser line) equipped with ZEN 2009 software for operation and X-Cite 120Q as the light source. Images were processed using ImageJ software (NIH) for background subtraction and measurement of absolute fluorescence intensities.

Protein labeling

NA and pA/G were conjugated with NHS-rhodamine according to the protocol provided by Thermo Fisher. Briefly, NHS-rhodamine adjusted to 10 mg/mL in DMSO was added in 10-fold mole excess to 5 mg/mL of protein in 1X PBS. The solution was thoroughly mixed and stored for a minimum of 2 h at 10°C. Following incubation, unreacted NHS-rhodamine was removed by gravity filtration using a PD-10 desalting column (GE Healthcare, USA), after which the recovered conjugate was concentrated by centrifugation (2000 x *g*) using a Amicon Ultra (3k, mwco) (MilliporeSigma, USA) filtration unit. Protein determination (Quick-start dye reagent, BioRad, USA) and UV-vis spectroscopy of conjugates were then conducted to determine final protein concentration and labeling efficiency. Regardless of the protein labeled, rhodamine:protein mole ratios consistently ranged from 2-3.

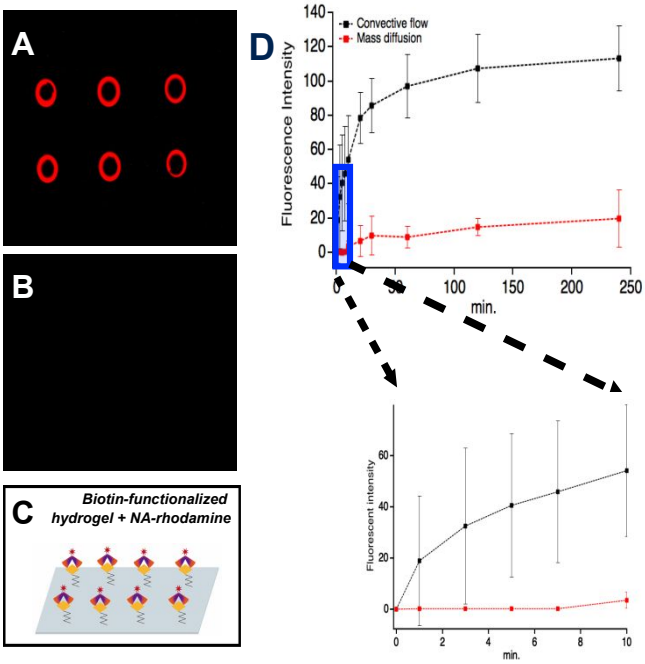

Figure 2 (A) Fluorescent image in the x-y plane (proximal to glass slide) of PEG-DA (20% (w/w)/AC-PEG-Biotin hydrogel (0.5% (w/w)) posts rehydrated in PBS containing 0.2 mg/mL NA-rhodamine (top panel, 50 ms exposure acquired 5 min. subsequent to initiation of reaction) and (B) 0.65 mg/mL pA/G-rhodamine (bottom panel, 500 ms exposure). (C) Schematic highlighting fluorescence capture at outer post surfaces via biotin-NA binding interactions. (D) Comparison of convective flow-mediated capture rate to rate obtained for mass diffusion. Both plots are the average of 3 replicate assays and error bars have been removed so as to highlight the differences in responses.

Results and discussion

The protocol adopted for conducting rehydration-mediated convective flow assays entailed the injection of PBS solution containing rhodamine-conjugated protein analyte into a PDMS chamber affixed to a glass slide upon which an array of functionalized hydrogel posts had been fabricated and dried (Fig 1A). As shown in the schematic, a second PDMS chamber positioned atop the chamber housing pre-polymer solution delivers a steady stream of N_2 for the purging of O_2 during post fabrication. This measure serves to minimize incomplete polymerization upon UV exposure and

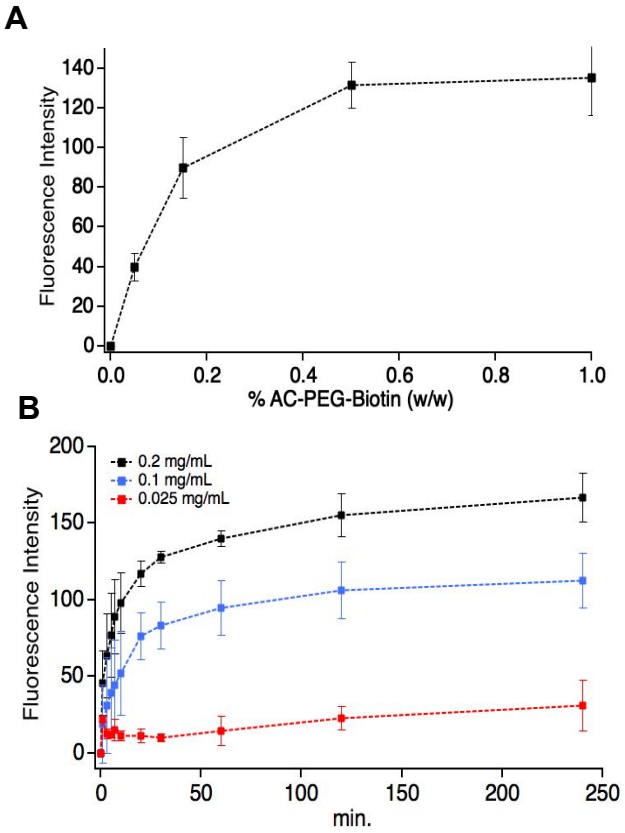

Figure 3 Impact of PEG-DA and AC-PEG-Biotin pre-polymer stoichiometry (A) on NA-rhodamine capture and detection. (B) Detection rates for range of NA-rhodamine concentrations. Plot A was derived from a single assay for each concentration of AC-PEG-Biotin tested and plot B is the average of 3 replicate assays for each concentration NA-rhodamine tested.

thereby maximize the structural integrity of microfabricated hydrogel posts. It is well established that dissolved O_2 is consumed by photoinitiator in a reaction that generates free radicals and peroxides that inhibit photopolymerization due to the inactivation of acrylate groups .[64,65] Studies conducted in our laboratory have demonstrated that N_2 purging mitigates this effect by reducing the influx of O_2 diffusion from PDMS into solution during photopolymerization.[17,66,24, 67] Subsequent to injection, fluorescent images were then acquired for protein analyte recognition over time

by monitoring the relative rate of binding at the hydrogel post structures both during and following rehydration. The schematic shown in Fig. 1B is an idealized representation of the underlying principle of the assay in which a fluorophore-conjugated Ab bound to antigen is transported to the surface of an Ab-functionalized hydrogel post for capture by rehydration-mediated convective flow forces in a sandwich immunoassay format.

The results acquired for a typical convection assay using posts fabricated with PEGDA and AC-PEG-Biotin, and NA-rhodamine as reporter analyte are shown in Fig. 2A. For each post viewed in the x-y plane, intense fluorescence is localized along their circumference following extensive washing with buffer, which is indicative of NA-biotin binding at the outer post surface and restricted penetration to the post interior. This observation is consistent with structures having an average mesh size of 2.4 nm, which was calculated based on the concentration of macromers in the pre-polymer solution using Flory-Rehner calculations as described in Zustiak and Leach [68] and is predicted to effectively exclude the uptake of proteins with larger hydrodynamic radii (ie. NA, M_w 60 kDa, R_{HYD} 7 nm).[69] This measurement has been reaffirmed using additional fluorophore conjugates of globular proteins ranging in size that are predicted to either exhibit uptake or exclusion by posts upon rehydration (see electronic supplementary information, Fig. S1). The absence of non-specific protein binding was confirmed using pA/G-rhodamine as reporter (Fig. 2B), as well as NA-rhodamine blocked with saturating levels of biotin prior to its use in the assay (data not shown).

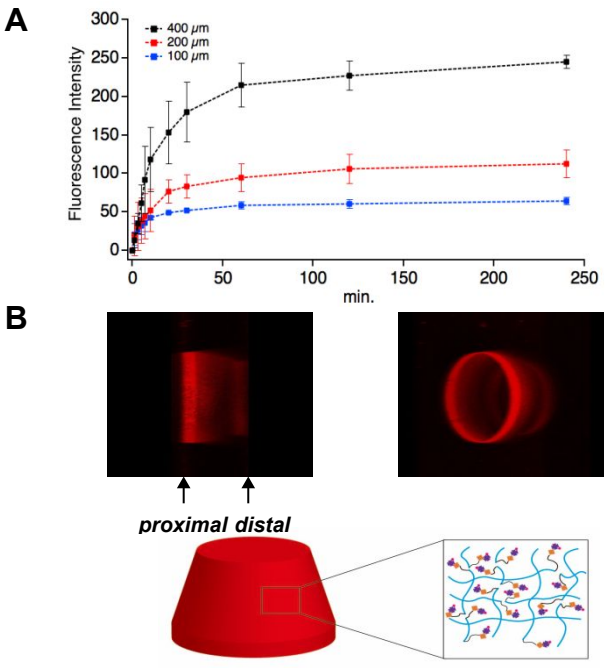

Figure 4 (A) Plot of NA-rhodamine detection over time for hydrogel posts varying in diameter. The plot for each diameter is the average of 3 replicate assays. (B) 3-D confocal scanning images of PEG-DA/AC-PEG-Biotin post incubated with NA-rhodamine. In the left image, the post has been rotated 90° with respect to the z axis and in the right image, the post is rotated an additional 45°. Images were assembled from point scanning of 2.5 μm interval slices along the z axis using a 10X objective and a dwell time of 5.8 μs.

Fig. 2D summarizes the kinetics of convective flow-mediated NA binding over 4 h, which exhibits a hyperbolic response highlighted by an initial rapid rate of analyte recognition that transitions to a greatly reduced rate at ~10-15 min following post rehydration. First derivative calculations of the slope for each *x* value of the plot show the highest slope value at 1 min. (i.e. 19.25), which diminishes over the time course according to a *ln* function (e.g. slope of 0.08 at 4 h). In contrast, the kinetics of a mass diffusion control experiment performed in parallel is characterized as a second-order polynomial function with a slope of 0.18 at t = 1 min. that decreases to 0.06 at t = 4h. While it is difficult to ascertain the precise time at which binding facilitated by convective flow transitions to binding by mass diffusion, it can nevertheless be inferred from the plot inset that this occurs within approximately 6-8 min. following post rehydration. In addition to facilitating a rapid acceleration of assay time, it is suggestive from these data that convective flow, along with targeted improvements in experimental design parameters, can be effectively harnessed for capturing considerably more analyte by mitigating the effect of the temporally diminished concentration gradients that reflect analyte depletion and drive diffusive mass transfer. In developing an appropriate model for comparing the kinetics of NA binding by convective flow versus mass diffusion, the mass diffusion assay was conducted by first rehydrating posts in PBS buffer, after which the appropriate volume of NA-rhodamine required for matching the concentration used in the convection assay was injected into the chamber. Gentle mixing of the chamber subsequent to the delivery of NA-rhodamine ensured a uniform concentration of NA-rhodamine.

In efforts to assess parameters that limit convection-driven assay performance, the effects that changes in the matrix density of biotin have on the relative level of NA capture were measured in a series of assays using hydrogels posts synthesized with 20% (w/w) PEGDA 700 and varying concentrations of AC-PEG-Biotin. The summary of these results (Fig. 3A) shows that NA capture, as indicated by relative fluorescence intensity, rises as the concentration of biofunctional macromer is increased in pre-polymer solution and that a maximum is achieved at a concentration of ~0.5% (w/w). This demonstrates the necessity of pre-determining an optimal formulation for relative macromer concentration, which facilitates enhanced detection sensitivity by virtue of maximizing the availability of analyte recognition elements and/or minimizing diminished analyte recognition due to steric hindrance considerations. Subsequent detection sensitivity experiments utilizing hydrogel posts synthesized in accordance with this formulation exhibited fluorescence intensity profiles that reflect a roughly linear capture response with respect to a range of NA-rhodamine concentrations tested (Fig. 3B).

To identify additional assay parameters that can be tuned to improve detection sensitivity, hydrogel posts synthesized with varying diameters, and therefore differences in volume and functional surface area, were tested in convective flow assays. Fig 4A

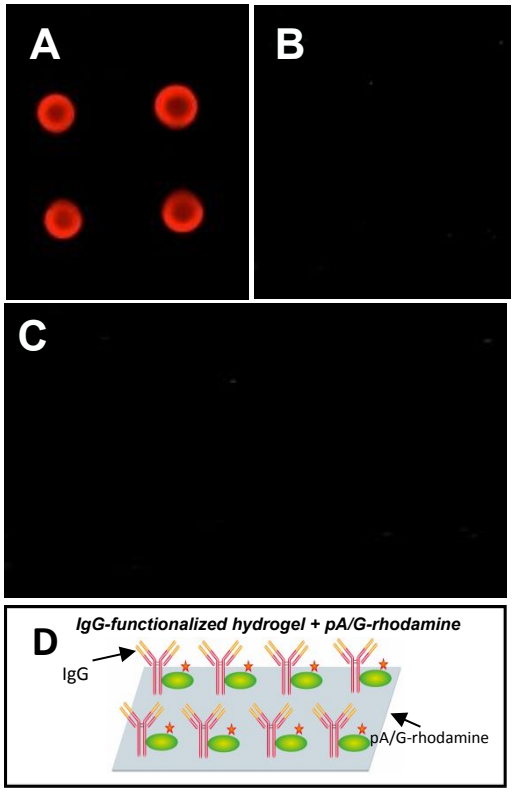

Figure 5 (A) Fluorescent image of PEG-DA (20% (w/w))/AC-PEG-NHS (1% (w/w)) hydrogel posts functionalized with IgG and rehydrated in PBS containing 0.65 mg/mL pA/G-rhodamine (500 ms exposure acquired 5 min. subsequent to initiation of reaction). (B) Image of non-functionalized PEG-DA/AC-PEG-NHS posts rehydrated in PBS containing 0.65 mg/mL pA/G-rhodamine (500 ms exp.). (C) Image of IgG functionalized HG posts rehydrated in PBS containing 0.1 mg/mL NA-rhodamine(500 ms exp.). (D) Schematic of IgG/Pro-AG assay.

summarizes the performance of hydrogel posts with diameters of 100 µm, 200 µm and 400 µm, and shows that fluorescence intensity measurements for images captured in the x-y plane scale proportionately with changes in post diameter. Similar results were obtained using posts synthesized with a diameter of 200 µm in PDMS chambers of varying depths (data not shown). Detailed imaging, however, of 200 µm diameter hydrogel posts using point-scanning confocal microscopy confirmed the reproducible fabrication of truncated structures of ~140 µm in height that are convex at their distal termini and display a progressively diffuse decoration of fluorescence along the z-axis subsequent to incubation with NA-rhodamine (Fig. 4B). This is suggestive of a reduction in the biotin-functionalized matrix density that is attributed, to some extent, to an attenuation in UV intensity at increasing distance from the glass slide support for anchored post fabrication. However, based on reports quantifying hydrogel photopolymerization in droplets[70] and between PDMS planes,[71] attenuated hydrogel formation is a consequence of the interplay of several factors, including UV power, UV exposure, time and the inhibitory effect of O_2 on macromer polymerization that is persistent despite N_2 purging. The collective effect of spatially varying these parameters accounts for both the tapered post shape and the reduction in acryl conversion, and therefore biotin incorporation, within the hydrogel network. A more complete model of these variables will thereby establish experimental conditions that can be tuned for fabricating hydrogel post structures with micro-architectural design features that enhance bioanalyte detection.

Finally, the potential versatility of convective flow-mediated hydrogel assays for enabling a range of biosensing applications was demonstrated using Ab grafted posts. In this study, assays were conducted using posts synthesized from pre-polymer solution containing 20% (w/w) PEGDA 700 and 1% (w/w) AC-PEG-NHS. Following fabrication and extensive washing to remove unreacted macromers, post fabrication entailed incubation with purified rabbit IgG to form stable amide bonds via the reaction of NHS groups and the primary amines of IgG, and then treatment with ethanolamine to block unreacted NHS groups. A typical image acquired for assays using IgG-functionalized posts and pA/G-rhodamine as reporter shows, as is also shown using biotin-functionalized posts, intense fluorescence concentrated at the exterior surface. In contrast, however, penetration to the post interior is more evident. This suggests a higher level of porosity or could also be rationalized by the lower M_w of pA/G (i.e. 47.5 kDa) with respect to NA. The absence of non-specific surface interactions was demonstrated using non-functionalized posts and pA/G-rhodamine as reporter (Fig. 5B), as well as IgG-functionalized posts using NA-rhodamine reporter (data not shown).

Conclusions

The findings of this study demonstrate the feasibility of a novel and facile approach for rapid analyte detection that is based on the rehydration of microfabricated hydrogels and concomitant convective flow-mediated delivery of target analyte to recognition elements. Having been demonstrated via ligand recognition and fluorescent reporting, the versatility of this platform will enable practical enhancement to immunoassay platforms that employ antibodies, aptamers, antibody fragments, or other engineered proteins for the sensitive detection of target antigens in clinically relevant biological matrices. Based on studies conducted to critically evaluate the impact of functional design metrics on hydrogel capture of a model analyte, opportunites to significantly improve detection have been elucidated.[14, 41, 72-74] Most notable is the necessity to micro-engineer increases in effective surface area capture via the development of hydrogel matrices with controlled pore dimensions for selective analyte uptake and/or binding,[75,41] as well as the entrapment of functionalized, analyte-recognition nanoparticles within hydrogel scaffolds.[72,14,73] Incremental improvements in assay detection sensitivity are also likely to be achieved by scaling the optimal test volumes of analyte required for hydrogel rehydration and quantitative analyte recognition, thereby mitigating the extent to which mass diffusion limits the kinetics of an assay reaction.

Conflicts of interest

There are no conflicts to declare.

Acknowledgements

This work was funded by the NSF Faculty CAREER Program (BBBE 1254608), by the NIH-funded Wyoming IDeA Networks of Biomedical Research Excellence program (P20GM103432), and the National Institute of General Medical Sciences of the National Institutes of Health (P20GM121310). The authors also acknowledge support from the University of Wyoming School of Energy Resources (SER) and the Wyoming Engineering Initiative.

Notes and references

1. Kozel TR, Burnham-Marusich AR. Point-of-Care Testing for Infectious Diseases: Past, Present, and Future. *Journal of Clinical Microbiology*. 2017;**55**(8):2313.
2. Symul L, Wac K, Hillard P, Salathé M. Assessment of menstrual health status and evolution through mobile apps for fertility awareness. *NPJ digital medicine*. 2019;**2**(1):1-10.
3. Ferretti L, Wymant C, Kendall M, Zhao L, Nurtay A, Abeler-Dörner L, et al. Quantifying SARS-CoV-2 transmission suggests epidemic control with digital contact tracing. *Science*. 2020:eabb6936.
4. He J. Chapter 5.1 - Practical Guide to ELISA Development. In: Wild D, editor. The Immunoassay Handbook (Fourth Edition). Oxford: Elsevier; 2013. p. 381-93.
5. Lequin RM. Enzyme Immunoassay (EIA)/Enzyme-Linked Immunosorbent Assay (ELISA). *Clinical Chemistry*. 2005;**51**(12):2415-8.
6. Visaveliya N, Lenke S, Köhler JM. Composite Sensor Particles for Tuned SERS Sensing: Microfluidic Synthesis, Properties and Applications. *ACS Applied Materials & Interfaces*. 2015;**7**(20):10742-54.
7. Kukushkin VI, Ivanov NM, Novoseltseva AA, Gambaryan AS, Yaminsky IV, Kopylov AM, et al. Highly sensitive detection of influenza virus with SERS aptasensor. *PLOS ONE*. 2019;**14**(4):e0216247.
8. Yetisen AK, Akram MS, Lowe CR. Paper-based microfluidic point-of-care diagnostic devices. *Lab on a Chip*. 2013;**13**(12):2210-51.
9. Li H, Steckl AJ. Paper Microfluidics for Point-of-Care Blood-Based Analysis and Diagnostics. *Analytical Chemistry*. 2019;**91**(1):352-71.
10. Hosseini S, Vázquez-Villegas P, Rito-Palomares M, Martinez-Chapa SO. Advantages, Disadvantages and Modifications of Conventional ELISA. In: Hosseini S, Vázquez-Villegas P, Rito-Palomares M, Martinez-Chapa SO, editors. Enzyme-linked Immunosorbent Assay (ELISA): From A to Z. Singapore: Springer Singapore; 2018. p. 67-115.
11. Neng J, Harpster MH, Wilson WC, Johnson PA. Surface-enhanced Raman scattering (SERS) detection of multiple viral antigens using magnetic capture of SERS-active nanoparticles. *Biosensors and Bioelectronics*. 2013;**41**:316-21.
12. Deligkaris K, Tadele TS, Olthuis W, van den Berg A. Hydrogel-based devices for biomedical applications. *Sensors and Actuators B: Chemical*. 2010;**147**(2):765-74.
13. Hoffman AS. Hydrogels for biomedical applications. *Advanced Drug Delivery Reviews*. 2012;**64, Supplement**:18-23.
14. Gaharwar AK, Peppas NA, Khademhosseini A. Nanocomposite hydrogels for biomedical applications. *Biotechnol Bioeng*. 2014;**111**(3):441-53.
15. Wagner VE, Koberstein JT, Bryers JD. Protein and bacterial fouling characteristics of peptide and antibody decorated surfaces of PEG-poly(acrylic acid) co-polymers. *Biomaterials*. 2004;**25**(12):2247-63.
16. Benamer S, Mahlous M, Boukrif A, Mansouri B, Youcef SL. Synthesis and characterisation of hydrogels based on poly(vinyl pyrrolidone). *Nuclear Instruments and Methods in Physics Research Section B: Beam Interactions with Materials and Atoms*. 2006;**248**(2):284-90.
17. Krutkramelis K, Xia B, Oakey J. Monodisperse Polyethylene Glycol Diacrylate Hydrogel Microsphere Formation by Oxygen-Controlled Photopolymerization in a Microfluidic Device. *Lab on a Chip*. 2016.
18. Debroy D, Oakey J, Li D. Interfacially-mediated oxygen inhibition for precise and continuous poly(ethylene glycol) diacrylate (PEGDA) particle fabrication. *Journal of Colloid and Interface Science*. 2018;**510**:334-44.
19. Caló E, Khutoryanskiy VV. Biomedical applications of hydrogels: A review of patents and commercial products. *European Polymer Journal*. 2015;**65**:252-67.
20. Naahidi S, Jafari M, Logan M, Wang Y, Yuan Y, Bae H, et al. Biocompatibility of hydrogel-based scaffolds for tissue engineering applications. *Biotechnology Advances*. 2017;**35**(5):530-44.
21. Terray A, Oakey J, Marr DWM. Microfluidic Control Using Colloidal Devices. *Science*. 2002;**296**(5574):1841.
22. Jang J-H, Dendukuri D, Hatton TA, Thomas EL, Doyle PS. A Route to Three-Dimensional Structures in a Microfluidic Device: Stop-Flow Interference Lithography. *Angewandte Chemie International Edition*. 2007;**46**(47):9027-31.
23. Khan OF, Sefton MV. Endothelialized biomaterials for tissue engineering applications in vivo. *Trends in Biotechnology*. 2011;**29**(8):379-87.
24. LeValley PJ, Noren B, Kharkar PM, Kloxin AM, Gatlin JC, Oakey JS. Fabrication of Functional Biomaterial Microstructures by in Situ Photopolymerization and Photodegradation. *ACS Biomaterials Science & Engineering*. 2018;**4**(8):3078-87.
25. Ifkovits JL, Burdick JA. Review: Photopolymerizable and Degradable Biomaterials for Tissue Engineering Applications. *Tissue Engineering*. 2007;**13**(10):2369-85.
26. Nakayama Y, Ishikawa A, Sato R, Uchida K, Kambe N. Photodimerization and Polymerization of PEG Derivatives through Radical Coupling using Photochemistry of Dithiocarbamate. *Polymer Journal*. 2008;**40**(11):1060-6.
27. Zacchigna M, Cateni F, Drioli S, Bonora GM. Multimeric, Multifunctional Derivatives of Poly(ethylene glycol). *Polymers*. 2011;**3**(3).
28. Choi NW, Cabodi M, Held B, Gleghorn JP, Bonassar LJ, Stroock AD. Microfluidic scaffolds for tissue engineering. *Nature Materials*. 2007;**6**(11):908-15.
29. Van Vlierberghe S, Dubruel P, Schacht E. Biopolymer-Based Hydrogels As Scaffolds for Tissue Engineering Applications: A Review. *Biomacromolecules*. 2011;**12**(5):1387-408.
30. M B, Vadithya A, Chatterjee A. As A Review on Hydrogels as Drug Delivery in the Pharmaceutical Field. *International journal of pharmaceutical and chemical sciences*. 2012;**1**:642-61.
31. Gopi S, Amalraj A, Thomas S. Effective drug delivery system of biopolymers based on nanomaterials and hydrogels-a review. *Drug Des*. 2016;**5**(129):2169-0138.
32. LeValley PJ, Tibbitt MW, Noren B, Kharkar P, Kloxin AM, Anseth KS, et al. Immunofunctional photodegradable poly(ethylene glycol) hydrogel surfaces for the capture and release of rare cells. *Colloids and Surfaces B: Biointerfaces*. 2019;**174**:483-92.
33. Buenger D, Topuz F, Groll J. Hydrogels in sensing applications. *Progress in Polymer Science*. 2012;**37**(12):1678-719.
34. Le Goff GC, Srinivas RL, Hill WA, Doyle PS. Hydrogel microparticles for biosensing. *European Polymer Journal*. 2015;**72**:386-412.
35. Okay O. General Properties of Hydrogels. 61970. p. 1-14.
36. Annabi N, Nichol JW, Zhong X, Ji C, Koshy S, Khademhosseini A, et al. Controlling the porosity and microarchitecture of hydrogels for tissue engineering. *Tissue Eng Part B Rev*. 2010;**16**(4):371-83.
37. Lee AG, Beebe DJ, Palecek SP. Quantification of kinase activity in cell lysates via photopatterned macroporous poly(ethylene glycol) hydrogel arrays in microfluidic channels. *Biomedical Microdevices*. 2012;**14**(2):247-57.
38. Park S, Lee HJ, Koh W-G. Multiplex Immunoassay Platforms Based on Shape-Coded Poly(ethylene glycol) Hydrogel Microparticles Incorporating Acrylic Acid. *Sensors*. 2012;**12**(6):8426.
39. Al-Ameen MA, Li J, Beer DG, Ghosh G. Sensitive, quantitative, and high-throughput detection of angiogenic markers using shape-coded hydrogel microparticles. *Analyst*. 2015;**140**(13):4530-9.
40. Ikami M, Kawakami A, Kakuta M, Okamoto Y, Kaji N, Tokeshi M, et al. Immuno-pillar chip: a new platform for rapid and easy-to-use immunoassay. *Lab on a Chip*. 2010;**10**(24):3335-40.
41. Kasama T, Ikami M, Jin W, Yamada K, Kaji N, Atsumi Y, et al. Rapid, highly sensitive, and simultaneous detection of staphylococcal enterotoxins in milk by using immuno-pillar devices. *Analytical Methods*. 2015;**7**(12):5092-5.

42. Li H, Leulmi RF, Juncker D. Hydrogel droplet microarrays with trapped antibody-functionalized beads for multiplexed protein analysis. *Lab on a Chip*. 2011;**11**(3):528-34.
43. Murakami Y, Maeda M. DNA-Responsive Hydrogels That Can Shrink or Swell. *Biomacromolecules*. 2005;**6**(6):2927-9.
44. Lin G, Chang S, Hao H, Tathireddy P, Orthner M, Magda J, et al. Osmotic swelling pressure response of smart hydrogels suitable for chronically implantable glucose sensors. *Sensors and Actuators B: Chemical*. 2010;**144**(1):332-6.
45. Harmon ME, Tang M, Frank CW. A microfluidic actuator based on thermoresponsive hydrogels. *Polymer*. 2003;**44**(16):4547-56.
46. Peteu SF, Oancea F, Sicuia OA, Constantinescu F, Dinu S. Responsive Polymers for Crop Protection. *Polymers*. 2010;**2**(3).
47. Ullah F, Othman MBH, Javed F, Ahmad Z, Akil HM. Classification, processing and application of hydrogels: A review. *Materials Science and Engineering: C*. 2015;**57**:414-33.
48. Chai Q, Jiao Y, Yu X. Hydrogels for Biomedical Applications: Their Characteristics and the Mechanisms behind Them. *Gels*. 2017;**3**(1).
49. Ionov L. Hydrogel-based actuators: possibilities and limitations. *Materials Today*. 2014;**17**(10):494-503.
50. Banerjee H, Suhail M, Ren H. Hydrogel Actuators and Sensors for Biomedical Soft Robots: Brief Overview with Impending Challenges. *Biomimetics*. 2018;**3**(3).
51. Wu Y, Li P, Yang L, Liu J. Individual SERS substrate with core–satellite structure decorated in shrinkable hydrogel template for pesticide detection. *Journal of Raman Spectroscopy*. 2014;**45**(1):68-74.
52. Lifson MA, Carter JA, Miller BL. Functionalized Polymer Microgel Particles Enable Customizable Production of Label-Free Sensor Arrays. *Analytical Chemistry*. 2015;**87**(15):7887-93.
53. Nguyen E, Schwartz M, Murphy W. Biomimetic Approaches to Control Soluble Concentration Gradients in Biomaterials. *Macromolecular bioscience*. 2011;**11**:483-92.
54. Qu X, Zhang H, Chen H, Aldalbahi A, Li L, Tian Y, et al. Convection-Driven Pull-Down Assays in Nanoliter Droplets Using Scaffolded Aptamers. *Analytical Chemistry*. 2017;**89**(6):3468-73.
55. Driscoll AJ, Johnson PA. Numerical modeling of analyte diffusion and adsorption behavior in microparticle and nanoparticle based biosensors. *Chemical Engineering Science*. 2018;**184**:141-8.
56. Kuscu M, Akan OB. Modeling convection-diffusion-reaction systems for microfluidic molecular communications with surface-based receivers in Internet of Bio-Nano Things. *PLOS ONE*. 2018;**13**(2):e0192202.
57. Park H, Hwang MP, Lee KH. Immunomagnetic nanoparticle-based assays for detection of biomarkers. *Int J Nanomedicine*. 2013;**8**:4543-52.
58. van Reenen A, de Jong AM, den Toonder JMJ, Prins MWJ. Integrated lab-on-chip biosensing systems based on magnetic particle actuation – a comprehensive review. *Lab on a Chip*. 2014;**14**(12):1966-86.
59. Cordeiro M, Ferreira Carlos F, Pedrosa P, Lopez A, Baptista VP. Gold Nanoparticles for Diagnostics: Advances towards Points of Care. *Diagnostics*. 2016;**6**(4).
60. Farka Z, Juřík T, Kovář D, Trnková L, Skládal P. Nanoparticle-Based Immunochemical Biosensors and Assays: Recent Advances and Challenges. *Chemical Reviews*. 2017;**117**(15):9973-10042.
61. Jiang Z, Xia B, McBride R, Oakey J. A microfluidic-based cell encapsulation platform to achieve high long-term cell viability in photopolymerized PEGNB hydrogel microspheres. *Journal of Materials Chemistry B*. 2017;**5**(1):173-80.
62. Majima T, Schnabel W, Weber W. Phenyl‐2,4,6‐trimethylbenzoylphosphinates as water‐soluble photoinitiators. Generation and reactivity of O=Ṗ(C6H5)(O−) radical anions. *Die Makromolekulare Chemie*. 2003;**192**:2307-15.
63. Xia Y, Whitesides GM. SOFT LITHOGRAPHY. *Annual Review of Materials Science*. 1998;**28**(1):153-84.
64. Höfer M, Moszner N, Liska R. Oxygen scavengers and sensitizers for reduced oxygen inhibition in radical photopolymerization. *Journal of Polymer Science Part A: Polymer Chemistry*. 2008;**46**(20):6916-27.
65. Ligon SC, Husár B, Wutzel H, Holman R, Liska R. Strategies to Reduce Oxygen Inhibition in Photoinduced Polymerization. *Chemical Reviews*. 2014;**114**(1):557-89.
66. Xia B, Krutkramelis K, Oakey J. Oxygen-Purged Microfluidic Device to Enhance Cell Viability in Photopolymerized PEG Hydrogel Microparticles. *Biomacromolecules*. 2016;**17**(7):2459-65.
67. Xia B, Jiang Z, Debroy D, Li D, Oakey J. Cytocompatible cell encapsulation via hydrogel photopolymerization in microfluidic emulsion droplets. *Biomicrofluidics*. 2017;**11**(4):044102.
68. Zustiak SP, Leach JB. Hydrolytically Degradable Poly(Ethylene Glycol) Hydrogel Scaffolds with Tunable Degradation and Mechanical Properties. *Biomacromolecules*. 2010;**11**(5):1348-57.
69. Perrault SD, Chan WCW. In vivo assembly of nanoparticle components to improve targeted cancer imaging. *Proceedings of the National Academy of Sciences*. 2010;**107**(25):11194-9.
70. Debroy D, Li-Oakey KD, Oakey J. Engineering functional hydrogel microparticle interfaces by controlled oxygen-inhibited photopolymerization. *Colloids and Surfaces B: Biointerfaces*. 2019;**180**:371-5.
71. Dendukuri D, Panda P, Haghgooie R, Kim JM, Hatton TA, Doyle PS. Modeling of Oxygen-Inhibited Free Radical Photopolymerization in a PDMS Microfluidic Device. *Macromolecules*. 2008;**41**(22):8547-56.
72. Schexnailder P, Schmidt G. Nanocomposite polymer hydrogels. *Colloid and Polymer Science*. 2009;**287**(1):1-11.
73. Zhao F, Yao D, Guo R, Deng L, Dong A, Zhang J. Composites of Polymer Hydrogels and Nanoparticulate Systems for Biomedical and Pharmaceutical Applications. *Nanomaterials*. 2015;**5**(4).
74. Neng J, Xu K, Wang Y, Jia K, Zhang Q, Sun P. Sensitive and Selective Detection of New Red Colorant Based on Surface-Enhanced Raman Spectroscopy Using Molecularly Imprinted Hydrogels. *Applied Sciences*. 2019;**9**:2672.
75. Lee Y, Lee HJ, Son KJ, Koh W-G. Fabrication of hydrogel-micropatterned nanofibers for highly sensitive microarray-based immunosensors having additional enzyme-based sensing capability. *Journal of Materials Chemistry*. 2011;**21**(12):4476-83.